ACS APPLIED MATERIALS & INTERFACES

Research Article

www.acsami.org

A 2D DNA Lattice as an Ultrasensitive Detector for Beta Radiations

Sreekantha Reddy Dugasani,[†,‡] Jang Ah Kim,[‡,§] Byeonghoon Kim,[†,‡] Pranav Joshirao,[∥] Bramaramba Gnapareddy,[†,‡] Chirag Vyas,[∥] Taesung Kim,*[,‡,§] Sung Ha Park,*[,†,‡] and Vijay Manchanda*[,∥,⊥]

[†]Department of Physics, [‡]Sungkyunkwan Advanced Institute of Nanotechnology (SAINT), [§]School of Mechanical Engineering, [∥]Department of Energy Science, and [⊥]School of Electronics and Electrical Engineering, Sungkyunkwan University, Suwon 440-746, Korea

Supporting Information

ABSTRACT: There is growing demand for the development of efficient ultrasensitive radiation detectors to monitor the doses administered to individuals during therapeutic nuclear medicine which is often based on radiopharmaceuticals, especially those involving beta emitters. Recently biological materials are used in sensors in the nanobio disciplines due to their abilities to detect specific target materials or sites. Artificially designed two-dimensional (2D) DNA lattices grown on a substrate were analyzed after exposure to pure beta emitters, ^{90}Sr-^{90}Y. We studied the Raman spectra and reflected intensities of DNA lattices at various distances from the source with different exposure times. Although beta particles have very low linear energy transfer values, the significant physical and chemical changes observed throughout the extremely thin, ~0.6 nm, DNA lattices suggested the feasibility of using them to develop ultrasensitive detectors of beta radiations.

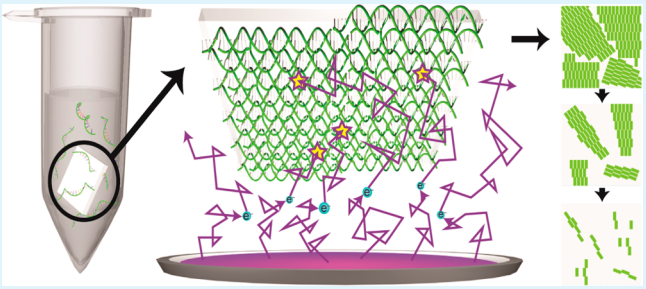

KEYWORDS: *DNA, nanotechnology, self-assembly, Raman, reflectance, radiation detector*

1. INTRODUCTION

Ionizing radiations are emitted by natural and man-made sources. The average worldwide effective dose received by human beings from natural sources is 2.4 mSv/y.[1] Apart from fallout due to nuclear weapons, major man-made sources of ionizing radiation are nuclear reactors, fuel cycle facilities, accelerators, industrial radiography, radiation processing units, and nuclear medicine (employed for diagnostic and therapeutic applications). The International Commission on Radiological Protection (ICRP) has prescribed an annual limit for all man-made sources as 1 mSv, where the contribution of medical radiation is most significant (40−1000 μSv/y) vis-à-vis other man-made sources (<1 μSv/y).[2,3] There is widespread interest in the accurate measurement of this dose to avoid over exposure during therapeutic radiation treatment. There is also concern about the irradiation of adjoining normal tissues while carrying out radiation treatment of the affected part of any organ. The depth dose as a function of thickness should ideally be of a rectangular shape with a flat maximum and a rapid disappearance of the trailing edges. This dose is computed by different codes and is verified using solid state dosimeters based on thermoluminescent dosimeters (TLD) or optically stimulated luminescence dosimeters (OSLD). Inorganic materials commonly employed in a TLD are LiF:Mg, $CaSO_4$:Dy, and CaF_2:Dy, and in an OSLD are Al_2O_3:C, BeO, and $LiMgPO_4$:Tb. These materials are chosen because of their tissue equivalence and relatively high sensitivity. Sensitivity of a TLD is around 100 μSv,[4] and for an OSLD it is around 10 μSv.[5] There is however a need to develop sensors which can respond to even lower doses (<10 μSv).[6] Since the therapeutic application of radiation is invariably based on beta particles (electrons) with linear energy transfer values much lower than those of alpha particles (helium nuclei), it is of particular interest to investigate ultrasensitive materials as sensors of beta radiations. The source of beta radiation used in the present work was ^{90}Sr which is in secular equilibrium with ^{90}Y. Among the isotopes used in intracoronary irradiation, ^{90}Sr−^{90}Y appears to be an ideal source.[7] ^{90}Sr decays to ^{90}Y, emitting a beta particle with a maximum kinetic energy of 0.546 MeV and a half-life of 28.7 years.[8] The daughter nucleus ^{90}Y, in secular equilibrium with its parent, decays to stable ^{90}Zr, emitting another beta particle with a maximum kinetic energy of 2.281 MeV with a half-life of 64.4 h.[8,9] The latter transition provides most of the therapeutically useful radiation in the irradiation process. Other accompanying fluorescent radiations (characteristic X-rays and Auger electrons) have very small probabilities of occurrence and low energies, and may therefore be disregarded.

Because they are structurally programmable, highly sensitive, and easily available, biomolecules, especially DNA molecules,

Received: December 4, 2013
Accepted: January 29, 2014
Published: January 29, 2014

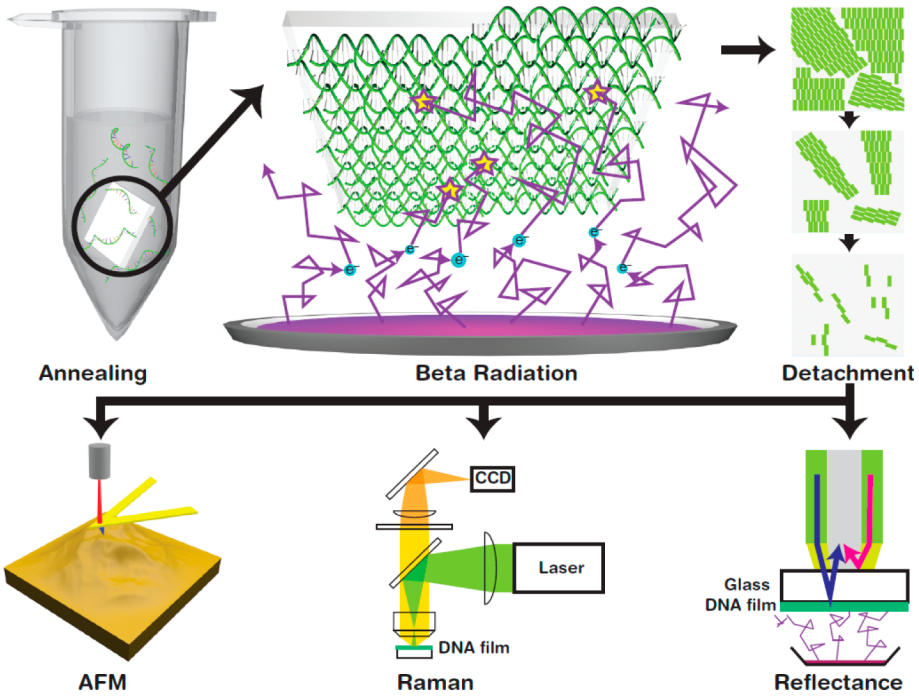

Figure 1. Schematics of annealing process for DNA lattice growth on a substrate by the surface assisted growth method; beta source emitting electrons with zigzag paths to DNA lattice; DNA lattice damage due to radiation bombardment; and measurement schematics of the AFM, Raman and reflectance spectroscopes.

are excellent candidates for use as sensing materials for beta radiations. The DNA molecule is an emerging bionanomaterial which has been explored for various applications such as biosensors,[10−12] photonics,[13] spintronics,[14] and nanoelectronics.[15,16] Most of these reports deal with analytes in the form of single or duplex DNA, but not as artificially designed two-dimensional (2D) polycrystalline nanostructures which can be made of tile-based DNA lattices on a substrate. Structural DNA nanotechnology has progressed over the three decades since its applicability to the construction of various dimensional structures made of DNA molecules.[17−19] Using the Watson−Crick complementary base-pairing rules, sequence-specific DNA strands are self-assembled into multiple DNA branches.[20,21] The reliable analysis of dimensional DNA nanostructures grown on various substrates could facilitate their application in physical devices, chemical sensors, and even in biomedicine. Additionally, it is convenient to fabricate artificially designed DNA nanostructures on functional substrates. In the present report, we demonstrate the feasibility of double-crossover (DX) tile-based 2D DNA lattices[22,23] as an ultrasensitive detector of beta radiation. The known diameter of the DNA duplex is 2 nm; however, a DNA duplex on the substrate has a diameter of 1.2 ± 0.2 nm under buffer, and 0.6 ± 0.2 nm in air due to the squeeze phenomenon which occurs with the charged substrate through electrostatic interactions.[24,25] The analysis of the beta radiation effect on a 2D DX DNA lattice was carried out using an atomic force microscope (AFM) in addition to a Raman spectroscope and an optical reflectance spectroscope.

2. EXPERIMENTAL PROCEDURE

Glass substrate with a size of 0.5 × 0.5 cm^2 was incubated in an O_2 plasma chamber (base pressure 5 × 10^{-2} Torr, working pressure ∼7.7 × 10^{-1} Torr, power 50 W, oxygen flow rate 45 sccm, and plasma generation time 5 min.), followed by rinsing with deionized (DI) water. The O_2 plasma-treated glass substrate was then utilized in a substrate assisted growth (SAG) annealing process.[26−29] Synthetic oligonucleotides, purified by HPLC, were purchased from Bioneer (Daejeon, Korea). Complexes were formed by mixing a stoichiometric quantity of each strand in 1 × TAE/Mg^{2+} (40 mM tris (hydroxymethyl) aminomethane (Tris), 1 mM ethylenediaminetetraacetic acid (EDTA; pH 8.0), 12.5 mM magnesium acetate). The concentration of individual oligonucleotides in the test tube was 70 nM. For annealing, the O_2 plasma-treated glass and the DNA strands were inserted into a test tube which was then placed in a Styrofoam box with 2 L of boiling water and subsequently cooled from 95 to 25 °C over a period of at least 24 h to facilitate the hybridization process. ^{90}Sr-^{90}Y, a pure beta source of 3.804 kBq, was procured from Eckert and Ziegler (Valencia, CA). Activity was distributed and evaporated on a polymeric membrane with a stainless steel backing. Aluminized mylar (0.9 mg/cm^2) was used as a cover. The active diameter of the beta standard source was 45 mm. Before beta exposure all the DNA samples were washed with DI water to remove the residues from surface and beta exposure was done under air.

For AFM imaging, a substrate-assisted grown sample was placed on a metal puck using instant glue. Buffer (10−20 μL of 1 × TAE/Mg^{2+}) was added to the substrate and an additional 5−10 μL of 1 × TAE/Mg^{2+} buffer was dispensed into the AFM tip (Veeco). AFM images were obtained with a Multimode Nanoscope (Veeco) in the liquid tapping mode.

Before measuring the Raman spectra of beta exposed samples, the unexposed samples were rinsed with DI water, followed by gentle blowing with nitrogen gas for removal of chemical residues from the DNA lattices on the O_2 plasma-treated glass substrate. After beta exposure, DNA samples were not washed with DI water. The measurements were performed at room temperature with a confocal Raman microscope (WITec, alpha 300 R) at 532 nm.

A reflectance probe (R600-8 UV−vis SR, Stellar Net) with seven optical fibers bundled around a 1600 μm fiber was utilized. For reflectance measurements, the six exterior fibers were illuminated by a light source (λ = 460 nm, WT&T). The interior fiber collected the reflected light and returned the signal to the spectrometer (AvaSepc-2048) and the photodetector (PDA36A-EC, Thorlab).

dx.doi.org/10.1021/am4055723 | ACS Appl. Mater. Interfaces 2014, 6, 2974−2979

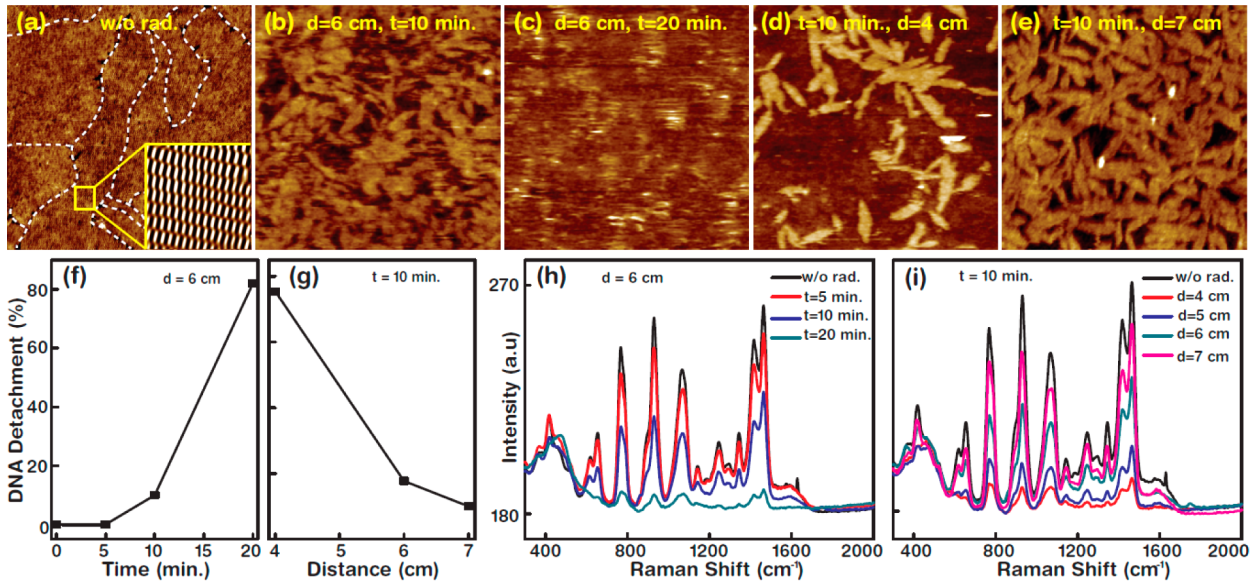

Figure 2. (a–e) AFM images of DNA lattices without and with irradiation. The scan size for all AFM images is 1 × 1 μm^2 unless otherwise noted. (a) Without radiation exposure, white dotted line indicates the crystal domain boundaries. The inset in the bottom right corner is a noise-filtered 2D Fourier transform spectrum showing the periodicity of the lattice (the scan size is 100 × 100 nm^2). Following DNA lattice radiation exposure from beta source (b, c) with t_{exp} = 10 and 20 min at constant d = 6 cm and (d, e) with d = 4 and 7 cm at constant t_{exp} = 10 min. (f, g) Detachment percentages as a function of t_{exp} at fixed d = 6 cm, and d at fixed t_{exp} = 10 min. (h, i) Variation of Raman band intensities for t_{exp} at constant d = 6 cm, and with distance d at constant t_{exp} = 10 min.

3. RESULTS AND DISCUSSION

The 2D DX DNA lattice used in this study consisted of two repeating DX tiles. A unit DX tile was organized in two DX junctions, and two parallel duplexes were tied up. Two kinds of DX tiles shown in Figure S1, Tables S1 and S2 in the Supporting Information (SI) were used for the construction of the 2D DNA lattice on the given substrate. The SAG method was used to fabricate a fully covered single layer with an extremely thin DNA lattice on an O_2-plasma-treated glass substrate. The thicknesses of the DNA lattice in solution, on glass under buffer, and on glass in air were ∼2.0, ∼1.2, and ∼0.6 nm, respectively. As mentioned, this variation was due to electrostatic attraction between the glass and DNA molecules. DNA crystallization, including random tile seeding, nucleation, and lattice growth was achieved using the SAG method, while the annealing process resulted in a monolayer DNA lattice with complete coverage controlled by the concentration of DNA molecules. Glass with complete coverage of 2D DX DNA polycrystalline lattices has advantages due to its transparency, which allows for the estimation of sensitivity through online monitoring via an optical fiber. The effect of beta radiation on DNA monolayers can be controlled by dosage which, for a given energy, depends on two physical parameters: the distance (d) between the radiation source and the DNA lattice, and the radiation exposure time (t_{exp}). Figure 1 shows experimental schematics of the DNA lattice growth on the substrate. Interestingly, beta particles do not travel in a straight path, but follow a zigzag path as they undergo collisions with molecules in the air. Beta particles emitted by ^{90}Y have a range of about 9 m, and those emitted by ^{90}Sr have a range of about 1.5 m in air.[30] However, the range is much less (∼10 mm) in denser materials including water and human tissues.[31,32]

Figure 2 shows typical AFM images, the detachment percentage, and the Raman spectra of the 2D DNA lattices after exposure to beta radiation at various d and t_{exp}. Figure 2a shows an AFM image of the lattices without radiation exposure, and an individual DX tile as constructed by noise-filtered 2D Fourier transform with dimensions of 12 nm × 4 nm is shown in the inset. Figure 2b and c shows DNA lattices for t_{exp} = 10 and 20 min at d = 6 cm. In Figure 2d and e, t_{exp} was fixed at 10 min and d was equal to 4 and 7 cm. Detachment of the DNA lattices due to exposure can clearly be identified in the AFM images for the shorter distance and longer exposure time. Figure 2f and g show the detachment percentages analyzed by AFM images in Figure S2 for t_{exp} = 0, 5, 10, 20 min at d = 6 cm, and d = 4, 6, 7 cm at t_{exp} = 10 min. It was interesting to observe that the deformation of the DNA lattices was significant when they were placed at a vertical distance of <4 cm from the ^{90}Sr-^{90}Y source even with short exposure time, 5 min. (results are not shown). There was a visible loss of adhesion of the lattices to the substrate when the distance was <4 cm and exposure time was ≥5 min. This is due to the large penetration range of the beta particles which caused the DNA lattices to deform, weakening the adhesion to the substrate. Recently, we have reported the possible use of a novel nanometric DNA thin film as a sensor for alpha radiations.[33] Extent of damage to the DNA film is a function of the absorbed energy (dose), and it is independent of the nature of radiations. It is difficult to make any direct comparison of the two radiations due to the following reasons: (i) Source strength for ^{90}Sr-^{90}Y (beta) is 3.804 KBq, whereas that for ^{241}Am (alpha) is 729 Bq. (ii) Average energy of emitted radiation for ^{90}Sr-^{90}Y is 0.471 MeV, whereas that for ^{241}Am is 5.48 MeV. (iii) Linear energy transfer value for beta radiations is much smaller and consequently the range in a given medium is much larger (few meters in air) as compared to the corresponding value (∼4.5 cm) for alpha radiations. Due to the difference in source strength and linear energy transfer value, optimum distance of the DNA lattices from radiation source was maintained as 4–7 cm in the present work.

dx.doi.org/10.1021/am4055723 | ACS Appl. Mater. Interfaces 2014, 6, 2974–2979

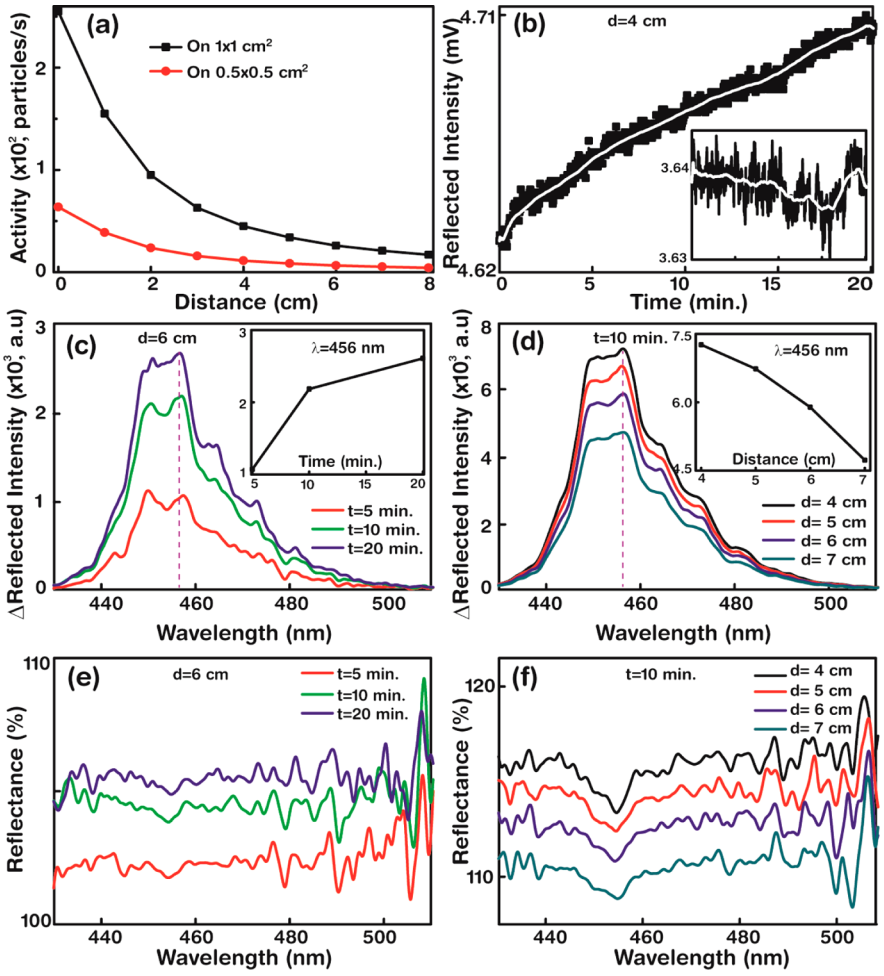

Figure 3. (a) Beta radiations fluence as a function of source-target distance. (b) Reflected light intensity upon beta radiation measured by the silicon photo detector at d = 4 cm for t_{exp} up to 20 min. Inset shows the reflected light intensity without DNA lattice. (c, d) Changes in reflected light intensity controlled by t_{exp} at d = 6 cm, and by d at t_{exp} = 10 min. (e, f) Reflectance as a function of wavelength with t_{exp} = 5, 10, and 20 min at fixed d of 6 cm, and with d = 4, 5, 6, and 7 cm at a fixed t_{exp} of 10 min.

The beta radiation effect on DNA lattices was also studied using Raman spectroscopic analysis for monitoring chemical bonds, and the results are shown in Figure 2h and i. Without radiation exposure, the DNA lattices showed the clear Raman bands of adenine, cytosine, guanine, thymine bases, and phosphate backbone groups with different modes of DNA molecules. The Raman bands observed were 1244, 1418 cm^{-1} (bending and stretching modes in adenine), 655, 1290, 1345 cm^{-1} (stretching modes in cytosine), 375, 623, 930, 1576 cm^{-1} (ring and stretching modes in guanine), 420, 780, 1290, 1465 cm^{-1} (ring and stretching modes in thymine), and 530, 1068, 1146 cm^{-1} (symmetric and stretching mode of phosphate backbone). The surface-enhanced Raman spectral peaks for each DNA base were demonstrated and the vibrational modes of DNA molecules immobilized on substrates were explained in previous literature.[34,35] The band assignments depicted in the Raman spectra in this report are in accordance with previous studies.[33−36] The beta radiation exposure effect on the DNA lattices at a constant d of 6 cm with t_{exp} equal to 5, 10, and 20 min, and at a constant t_{exp} of 10 min with d equal to 4, 5, 6, and 7 cm were analyzed. The systematic changes in the Raman spectra were clearly observable when d was varied between 4 and 7 cm, and the spectra showed gradual reductions in intensity of all peaks for the exposure of 10 min. With an increase in t_{exp} from 5 to 20 min at a constant d of 6 cm, there occurred a gradual suppression of all peaks which suggests chemical damage of the structural DNA lattices. The deformation damage increased as t_{exp} increased from 5 to 20 min for a fixed d of 6 cm, as well as with decreasing d from 7 to 4 cm at a fixed t_{exp} of 10 min.

It was possible to correlate the changes in the Raman spectra intensities with the beta particle fluence in the range from 10^3 to 10^4. Considering the average energy associated with each beta particle was 0.471 MeV (1/2 × (1/3 × 0.546 + 1/3 × 2.281)), the total kinetic energy of the incident particles was in the range from 7.54×10^{-11} to 7.54×10^{-10} J. However, in view of the nanometric thickness (~0.6 nm) of the DNA lattice and the low linear energy transfer value of beta radiation, only a small fraction of this energy could be absorbed. The range of ^{90}Y in polymethylmethaacrylate (PMMA), a tissue equivalent material obtained using a LiF-based TLD (effective atomic number of LiF is 8.1 compared to 7.4 for soft tissue), is ~10 mm.[31,32] Absorbed dose decreased from 286 mGy/MBq/h (1 mm from ^{90}Y source) to 56 mGy/MBq/h (2.17 mm from ^{90}Y source). The fraction of the energy absorbed in PMMA over 1.17 mm is ~80%. Considering DNA lattice used in the present work similar to PMMA, fraction of energy absorbed over ~0.6 nm (thickness of the DNA lattice) might be around 5×10^{-7}

dx.doi.org/10.1021/am4055723 | ACS Appl. Mater. Interfaces 2014, 6, 2974−2979

times the original energy. Theoretically, this absorbed energy is sufficient to break hydrogen bonds in the 69 base pairs of AT and the 79 base pairs of CG present in the unit DX lattice, (DX-1 + DX-2) (~6.13×10^{-18} J; see Figure S1 and quantitative description in the SI). Part of the energy might also be used to break the chemical bonds of the functional groups like phosphate, C−N and C═C of AT and CG. It is obvious that the damage and deformation observed by Raman spectra and AFM images are caused by the disruption of the DNA lattice, the rupture of a fraction of the chemical/hydrogen bonds, as well as physical damage caused by detachment of the DNA layers. Considering the total mass of the DNA lattice on a glass substrate (dimensions of 0.5 × 0.5 cm^2) was 33 ng (see the SI), and the beta radiation weighting factor of 1, the equivalent cumulative dose administered in 10 min varied between 0.2 and 2 μSv. Thus, the sensitivity of the DNA lattice is an order of magnitude better than that of OSLD materials and 2 orders of magnitude than that of TLD.

Figure 3a shows the fluence in Bq (per cm^2) of the DNA lattices on a glass substrate as a function of distance between the source and DNA lattices. It is obtained using a RAD Eye instrument incorporating a GM tube supplied by Thermo Fisher Scientific Messtechnik, GmbH, Germany which is based on ionization principles. The schematic of the fiber optic reflectance probe employed for the optical evaluation of the DNA lattice on exposure to a beta source is shown in Figure 1. This illustrates the multiple reflections occurring from the glass and the DNA lattice monolayer. When the incident light reaches the DNA lattice, a fraction of the light is reflected from the surface, while another fraction is absorbed, and the remaining is transmitted through the surface. The light reflected from the glass surface and the light passing through the DNA lattice was measured by a photodetector. Figure 3b shows the reflected intensity in millivolts, as measured by the photodetector, for an irradiation distance of 4 cm over a period of 20 min. The change in reflected light intensity upon beta radiation exposure was observed to be ~0.08 mV, which is appreciable considering background drift as ~0.01 mV, as shown in the inset of Figure 3b. For the control experiment, we measured the reflected intensities of a glass substrate immersed either in DI water or a normal DNA buffer 1 × TAE/Mg^{2+} as well as DNA lattices grown on a glass substrate without beta radiation exposure. As shown in Figure S3, similar intensities were observed for both DI water and buffer-treated glasses, but the DNA lattice showed lower intensities than the other samples. The reflected intensity changes of the DNA lattice recorded during exposure under various conditions are shown in Figure 3c and d. The insets represent the change in reflected intensity at a particular wavelength (λ = 456 nm). Figure 3e and f show the normalized reflectance percentage of beta-exposed DNA samples where the reflectance percentage is defined as the ratio of reflectance intensity with exposure (I) over the intensity without exposure (I_0) multiplied by 100, that is, (I/I_0) × 100. The resultant changes in the reflectance intensity of the DNA lattices at 456 nm, or changes in the intensity of the Raman spectra, were correlated with increasing fluence/dose. From these changes, we found that extremely thin DNA lattices can form the basis of a highly sensitive detector of beta radiation. It is interesting to note that, unlike solid state track detectors which can be used exclusively for quantification of heavy charged ions,[37] DNA lattices are versatile biomaterials which can detect various types of radiations effectively with high sensitivity.

4. CONCLUSION

In conclusion, we fabricated fully covered 2D DX DNA lattices on a glass substrate using the SAG method. After exposure to beta particles at various exposure times and distances, noticeable changes to morphology, the Raman spectra, and optical reflected intensities were observed. The Raman spectral peak intensities diminished by about 10 times with exposure to a beta source placed at a distance of 4 cm for 10 min. We correlated the changes in the AFM, Raman, and reflectance spectral behaviors with beta radiation fluence/dose which can provide the basis for the development of a sensitive detector or device for use in nanotechnology, biotechnology, and medicine as well as in more traditional disciplines such as physics, chemistry, and biology.

■ ASSOCIATED CONTENT

Supporting Information

Schematics of DNA sequences, Additional AFM images and reflectance spectra of DNA lattices and quantitative description of a double-crossover lattice. This material is available free of charge via the Internet at http://pubs.acs.org.

■ AUTHOR INFORMATION

Corresponding Authors

*E-mail: tkim@skku.edu (T.K.).
*E-mail: sunghapark@skku.edu (S.H.P.).
*E-mail: vkm25749@gmail.com (V.M.).

Notes

The authors declare no competing financial interest.

■ ACKNOWLEDGMENTS

This work was supported by the National Research Foundation of Korea (NRF) (2009-0083540, BSR Program) to T.K., 2012R1A2A2A01005985, MCR Program & 2009-0094023, BSR Program to S.H.P., and R31-2008-10029, WCU program to V.M. funded by the Ministry of Science, ICT & Future Planning, Korea (MSIP).

■ REFERENCES

(1) *Sources and Effects of Ionizing Radiation, Report to the General Assembly with scientific annexes*, UNSCEAR, United Nations, Vienna, Austria, annex B, 2000; Vol. *1*, p 112.
(2) *Sources and Effects of Ionizing Radiation, Report to the General Assembly with scientific annexes*, UNSCEAR, United Nations, Vienna, Austria, annex B, 2000; Vol. *1*, p 334.
(3) *Sources and Effects of Ionizing Radiation, Report to the General Assembly with scientific annexes*, UNSCEAR, United Nations, Vienna, Austria, annex B, 2000; Vol. *1*, p 194.
(4) Budzanowski, M.; Bilski, P.; Olko, P.; Ryba, E.; Perle, S.; Majewski, M. Dosimetric Properties of New Cards with High-Sensitivity MCP-N (LiF: Mg, Cu, P) Detectors for Harshaw Automatic Reader. *Radiat. Prot. Dosim.* **2007**, *125*, 251−255.
(5) Scarboro, S. B.; Followill, D. S.; Kerns, J. R.; White, R. A.; Kry, S. F. Energy Response of Optically Stimulated Luminescent Dosimeters for Non-reference Measurement Locations in a 6 MV Photon Beam. *Phys. Med. Biol.* **2012**, *57*, 2505−2515.
(6) *Dosimetry in diagnostic radiology: An international code of Practice, IAEA Technical Report*, Vienna, Austria, STI/PUB/1294, 2007; Vol. *457*, pp 1−359.
(7) Amols, H. I.; Zaider, M.; Weinberger, J.; Ennis, R.; Schiff, P. B.; Reinstein, L. E. Dosimetric Considerations for Catheter-based Beta and Gamma Emitters in the Therapy of Neo Intimal Hyperplasia in Human Coronary Arteries. *Int. J. Radiat. Oncol., Biol., Phys.* **1996**, *36*, 913−921.

(8) Radionuclide Transformations: Energy and Intensity of Emissions, *Int. Comm. Radiol. Prot. Publ.* **1983**, ICRP Publication 38, Ann ICRP 11−13.
(9) Dose and Volume Specification for Reporting Interstitial Therapy, *J. ICRU* **1997**, report 58.
(10) Nam, J. M.; Thaxton, C. S.; Mirkin, C. A. Nanoparticle-Based Bio-Bar Codes for the Ultrasensitive Detection of Proteins. *Science* **2003**, *301*, 1884−1886.
(11) Jung, J.; Kim, S. J.; Lee, K. W.; Yoon, D. H.; Kim, Y.; Kwak, H. Y.; Dugasani, S. R.; Park, S. H.; Kim, H. J. Approaches to Label-Free Flexible DNA Biosensors Using Low-Temperature Solution-Processed InZnO Thin-Film Transistors. *Biosens. Bioelectron.* **2014**, *55*, 99−105.
(12) Lu, Y.; Goldsmith, B. R.; Kybert, N. J.; Johnson, A. T. C. DNA-Decorated Graphene Chemical Sensors. *Appl. Phys. Lett.* **2010**, *97*, 083107−3.
(13) Lee, K.; Kim, K. M.; Lee, J.; Amin, R.; Kim, B.; Park, S. K.; Lee, S.; Park, S. H.; Kim, H. J. A Two-Dimensional DNA Lattice Implanted Polymer Solar Cell. *Nanotechnology* **2011**, *22*, 375202−6.
(14) Geert, L. J. A. R. A New Twist on Spintronics. *Science* **2011**, *331*, 864−865.
(15) Braun, E.; Eichen, Y.; Sivan, U.; Yoseph, G. B. DNA Templated Self-Assembly of a Conductive Wire Connecting Two Electrodes. *Nature* **1998**, *391*, 775−778.
(16) Rakitin, A.; Aich, P.; Papadopoulos, C.; Kobzar, Y.; Vedeneev, A. S.; Lee, J. S.; Xu, J. M. Metallic Conduction through Engineered DNA: DNA Nanoelectronic Building Blocks. *Phys. Rev. Lett.* **2001**, *86*, 3670−3673.
(17) Kallenbach, N. R.; Ma, R.-I.; Seeman, N. C. An Immobile Nucleic Acid Junction Constructed from Oligonucleotides. *Nature* **1983**, *305*, 829−831.
(18) Kallenbach, N. R.; Ma, R. I.; Veeneman, G. H.; van Boom, J. H.; Seeman, N. C. Fourth Rank Immobile Nucleic Acid Junctions. *J. Biomol. Struct. Dyn.* **1983**, *1*, 159−168.
(19) Amin, R.; Kim, S.; Park, S. H.; LaBean, T. H. Artificially designed DNA Nanostructures. *Nano* **2009**, *4*, 119−139.
(20) Wang, Y.; Mueller, J. E.; Kemper, B.; Seeman, N. C. Assembly and Characterization of Five-Arm and Six-Arm DNA Branched Junctions. *Biochemistry* **1991**, *30*, 5667−5674.
(21) He, Y.; Chen, Y.; Liu, H.; Ribbe, A. E.; Mao, C. Self-Assembly of Hexagonal DNA Two-Dimensional (2D) Arrays. *J. Am. Chem. Soc.* **2005**, *127*, 12202−12203.
(22) Fu, T. J.; Seeman, N. C. DNA Double-Crossover Molecules. *Biochemistry* **1993**, *32*, 3211−3220.
(23) Winfree, E.; Liu, F.; Wenzler, L. A.; Seeman, N. C. Design and Self-Assembly of Two-Dimensional DNA Crystals. *Nature* **1998**, *394*, 539−544.
(24) Park, S. H.; Prior, M. W.; LaBean, T. H.; Finkelstein, G. Optimized Fabrication and Electrical Analysis of Silver Nanowires Templated on DNA Molecules. *Appl. Phys. Lett.* **2006**, *89*, 033901−3.
(25) Mark, M.; Szczelkun, D.; Round, A. N.; Miles, M. J. Comparison Between Shear Force and Tapping Mode AFM - High Resolution Imaging of DNA. *Single Mol.* **2002**, *3*, 105−110.
(26) Hamada, S.; Murata, S. Substrate-Assisted Assembly of Interconnected Single-Duplex DNA Nanostructures. *Angew. Chem., Int. Ed.* **2009**, *48*, 6820−6823.
(27) Sun, X.; Ko, S. H.; Zhang, C.; Ribbe, A. E.; Mao, C. Surface-Mediated DNA Self-Assembly. *J. Am. Chem. Soc.* **2009**, *131*, 13248−13249.
(28) Dugasani, S. R.; Lee, N. H.; Lee, J.; Kim, B. H.; Hwang, S. U.; Lee, K. W.; Kang, W. N.; Park, S. H. Magnetic Characteristics of Copper Ion-Modified DNA Thin Films. *Sci. Rep.* **2013**, *3*, 1819.
(29) Kim, B.; Amin, R.; Lee, J.; Yun, K.; Park, S. H. Growth and Restoration of a T-Tile-Based 1D DNA Nanotrack. *Chem. Commun.* **2011**, *47*, 11053−11055.
(30) Annunziata, M. F. L. *Handbook of Radioactivity Analysis*, 3rd ed.; Elservier Science: Amsterdam, 2003.
(31) Soares, C. G.; Vynckier, S.; Jarvinen, H.; Cross, W. G.; Sipila, P.; Fluhs, D.; Schaeken, B.; Mourtada, F. A.; Bass, G. A.; Williams, T. T. Dosimetry of Beta-ray Ophthalmic Applicators: Comparison of Different Measurement Methods. *Med. Phys.* **2001**, *28*, 1373−1384.
(32) Tandon, P.; Malpani, B. L.; Venkatesh, M.; Bhatt, B. C. Estimation of Radiation Dose at Various Depths for Commonly Used Radionuclides in Radiosynoviorthesis in a Tissue Equivalent Material. *Med. Phys.* **2006**, *33*, 2744−2750.
(33) Kulkarni, A.; Kim, B.; Dugasani, S. R.; Joshirao, P.; Kim, J.; Vyas, C.; Manchanda, V.; Kim, T. S.; Park, S. H. A Novel Nanometric DNA Thin Film as a Sensor for Alpha Radiation. *Sci. Rep.* **2013**, *3*, 2062.
(34) Otto, C.; van den Tweel, T. J. J.; De Mu, F. F. M.; Greve, J. Surface-Enhanced Raman Spectroscopy of DNA Bases. *J. Raman Spectrosc.* **1986**, *17*, 289−298.
(35) Vasudev, M.; Wu, T. C.; Biswas, S.; Mitra, D.; Stroscio, M. A.; Guthrie, S.; Reed, M.; Burris, K. P.; Neal Stewart, C. Optoelectronic Signatures of DNA-Based Hybrid Nanostructures. *IEEE Trans. Nanotechnol.* **2011**, *10*, 35−43.
(36) Ponkumar, S.; Duraisamy, P.; Iyandurai, N. Structural Analysis of DNA Interactions with Magnesium Ion Studied by Raman Spectroscopy. *Am. J. Biochem. Biotechnol.* **2011**, *7*, 135−140.
(37) Kulkarni, A.; Vyas, C. K.; Kim, H.; Kalsi, P. C.; Kim, T. S.; Manchanda, V. Online Optical Monitor of Alpha Radiations Using a Polymeric Solid State Nuclear Track Detector CR-39. *Sens. Actuators, B* **2012**, *61*, 697−701.